Journal of Vibration Engineering & Technologies (2025) 13:577
https://doi.org/10.1007/s42417-025-02160-6

ORIGINAL PAPER

Integration of two Absorbers to Damp Two Distinct Modes Responsible for Two Different Types of Chatter in Grooving with Slender Blades

Danaram Jhakar[1] · **Mohit Law**[1]

Received: 13 June 2025 / Revised: 15 September 2025 / Accepted: 13 October 2025 / Published online: 30 October 2025

Abstract

Purpose Experimental analysis of grooving with slender blades reveals two chatter types: regenerative diametrical chatter and mode-coupling snaking chatter on the side walls, linked to two distinct vibration modes. Since grooving is a fixed width of cut operation, traditional stability diagrams offer little guidance for selecting chatter-free cutting parameters. Hence, the only feasible strategy is to damp the two modes responsible for contributing to chatter. Though blades exist to damp diametrical chatter, but no solution yet addresses the mode responsible for snaking chatter. This paper discusses a remedy for that problem by showing how two absorbers can be integrated within the blade.

Methods Classical analytical methods to tune absorbers assume that there is just one mode and one absorber that requires tuning. Since we require two to be tuned in different directions, we propose a new solution using multi-component receptance coupling. We treat the blade and absorbers as separate subsystems, then combine receptances to find absorber parameters that minimize the assembled system's response.

Results and. conclusions Model predictions show that the newly conceptualized blade can damp the peak amplitude of the in-plane bending mode by 53% and of the out-of-plane bending mode by 67%. The absorber parameters we identified are realistic, and the simulation-based results are promising. Together, these support the design, development, and prototyping of new damped blades with two integrated absorbers. Our methods are also easily extendable to other systems requiring the integration and tuning of multiple absorbers.

Keywords Grooving · Chatter · Absorber · Receptance coupling

Introduction

Machining of deep grooves requires the use of slender cantilevered blades. Since the blades are thin, they tend to vibrate when excited by cutting process forces. These process-induced excitations sometimes result in large amplitude unstable chatter vibrations that damage the blade and the surface of the grooves being machined. Since grooves are usually made to house seals and O-rings, no vibration marks are acceptable on the machined surfaces. Chatter must hence be avoided.

The usual method to avoid chatter is to select cutting parameters, namely the depth or width of cut together with the spindle speed that will result in stable cutting conditions. Selections are guided by analytically predicted stability diagrams. These diagrams have proven very useful for mitigating chatter in turning [1] and milling [2]. However, since grooving is a fixed width of cut operation, stability diagrams are of little use. Furthermore, stability diagrams can only characterize chatter of the regenerative type, i.e., chatter that occurs due to modulation of the chip thickness. However, as recent research has revealed [3], chatter in grooving can be of two types: diametrical chatter that is of the regenerative kind and snaking chatter on the side walls that is of the mode-coupling type. Since mode-coupling chatter is not completely understood yet [4, 5], models for it still cannot still prescribe stable grooving operations. Hence, the only feasible strategy for stable grooving operations is to damp the vibration mode(s) responsible for contributing to chatter.

✉ Mohit Law
mlaw@iitk.ac.in

[1] Machine Tool Dynamics Laboratory, Department of Mechanical Engineering, Indian Institute of Technology Kanpur, Kanpur 208016, India

Grooving involves feeding the blade into the workpiece to make grooves. Blades are stiffer along their length (l) than their height (h) and/or width (w). As such, the vibrations of the blade along its length are negligible and do not result in significant undulations on the diameter as the blade feeds into the workpiece. Instead, undulations on the diameter resulting in diametrical chatter are thought to occur due to the tangential and feed forces causing in-plane bending of the blade [6]. This mode, showing schematically in Fig. 1(a), is one of the two modes to be damped. The other mode to be damped is that along the blade's width. Though the blade is guided in the groove it is making, since the blade is significantly more flexible in its thickness direction, any perturbation during the process causes the blade to undergo bending vibrations in its thickness direction that result in undulations on the side walls of the groove being machined. These undulations are also shown schematically in Fig. 1(b). Since the blade cuts a new surface on the side walls as it advances in the feed direction, there is no regeneration action on the side walls, and the undulations resulting in snaking chatter are thought to be of the mode-coupling type, i.e., when the cutting forces simultaneously

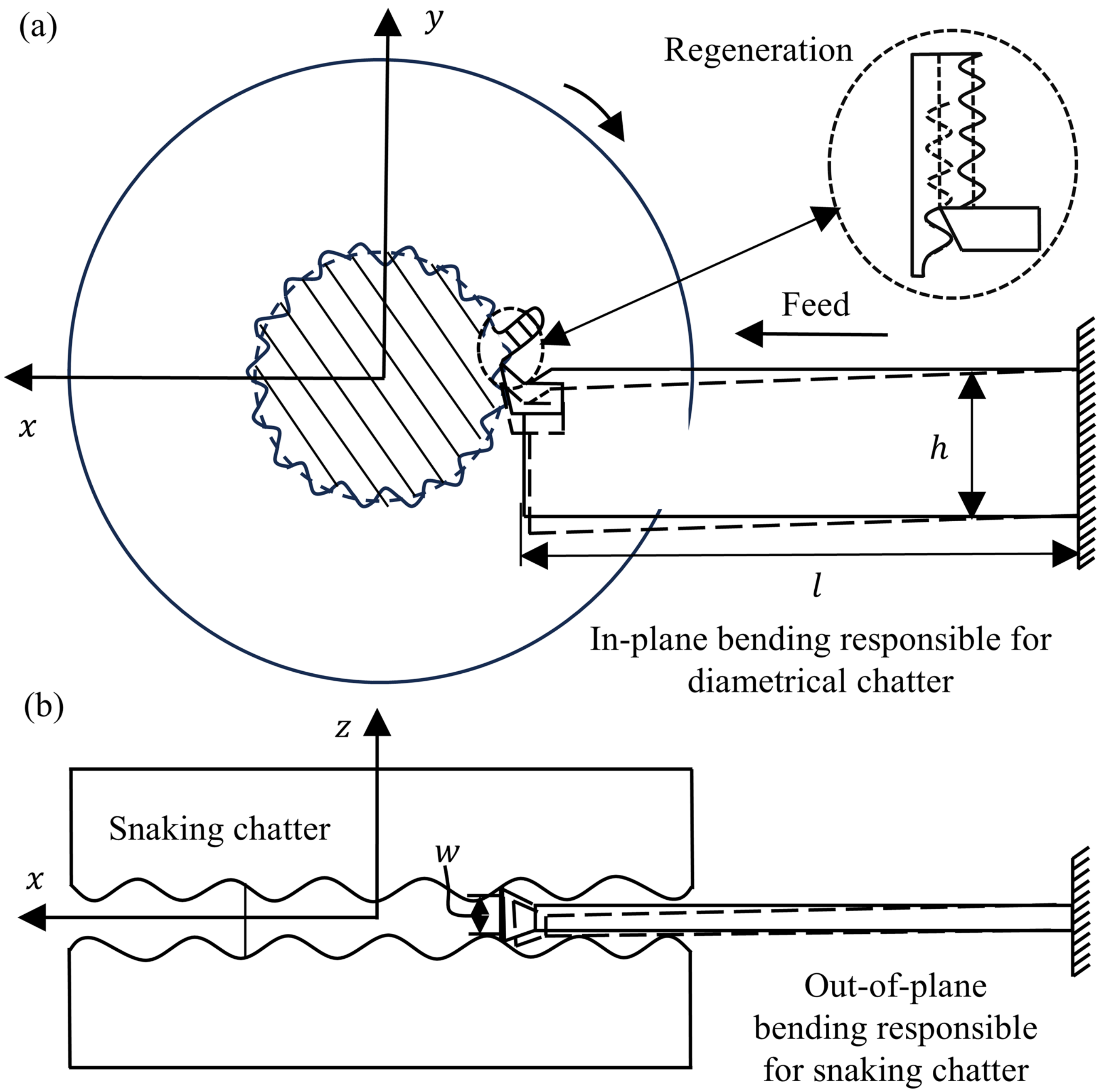

Fig. 1 Schematic of deep grooving with a slender cantilevered blade resulting in (**a**) diametrical chatter, and (**b**) snaking chatter

cause in-plane and out-of-plane bending of the blade [3]. Hence, the two modes to be damped are the modes causing in-plane and out-of-plane bending of the grooving blade.

Damping of tool vibration modes is most easily done by integrating tuned mass absorbers within tools. The idea is to place an absorber within the tool such that when the tool vibrates, it transfers those vibrations to the absorber [7–10]. The absorber is usually supported in O-rings and tuning it includes selecting an appropriate mass of the absorber and adjusting the stiffness and damping properties of the elastomeric O-rings that support it.

Classical analytical methods to tune absorbers assume that there is just one mode and one absorber that requires tuning [11, 12]. These classical methods were indeed used to integrate a tuned absorber within a grooving blade to damp the mode responsible for diametrical chatter [6], and for tuning single absorbers to damp the mode responsible for chatter in turning and boring applications [8–10]. To further improve damping performance, researchers also reported on the success of tuning multiple tuned mass dampers to damp the same target mode. For example, in [13], three tuned mass dampers were integrated to damp one target mode responsible for chatter, and in [14, 15], two tuned mass dampers were integrated to damp the mode of interest. In all these cases only one mode was sought to be damped, and in every case, the tuned mass damper(s) were oriented along the same direction as the mode which was to be damped.

Since deep grooving has two distinct vibration modes in two different directions that are responsible for the two types of chatter that is observed [3], the standard methods of tuning absorbers are not applicable, and there is a need for a different method to integrate, design, and tune two absorbers. Developing and demonstrating the workings of such a framework is the main aim and new scientific and technical contribution of the research reported in this paper.

To integrate two tuned absorbers within the blade, we leverage the strengths of the receptance coupling approach. Receptances are frequency response functions (FRFs) that represent the system's dynamics by characterizing the relationship between output displacements and input forces as a function of frequency. The receptance coupling approach is a structural modification tool used to couple two separate subsystems in the frequency domain using their individual component level receptances. The approach has found much use in machine tool applications to predict tool point dynamics [16–18], as well as in some automotive applications [19]. Recent work has also shown how the method can be used to design absorbers to damp machine tool structural vibrations [20] and to tune a tune a single absorber integrated within a boring bar [21]. Relevant recent research has also shown how two tuned mass dampers can be designed using the receptance coupling approach to suppress two orthogonal vibration modes of a micro-end mill [22]. This paper will build on such previous successes.

The remainder of this paper is organized as follows: at first, we present conclusive experimental evidence of the two types of chatter observed in grooving being caused by two distinct vibration modes. In the next section, we discuss a potential design of a damped grooving blade with two absorbers integrated within it. In the section after, we present the receptance coupling framework to integrate two absorbers within the blade. Numerical investigations that follow show how both modes contributing to chatter can indeed be damped successfully. In the discussions section, we discuss the sensitivity of the results to key parameters and discuss design aspects that can guide prototyping. The paper is finally concluded with an outlook.

Experiments Showing Diametrical and Snaking Chatter

This section discusses experimental results to offer conclusive proof of two distinct grooving blade modes being responsible for the two different types of chatter that is observed. Experiments were conducted on a CNC turning machine with three blades. Two blades were thick, and one was thin. Results presented herein expand on our preliminary reports in [3] which were limited to only the thick blades. Of the two thick blades, one was a regular blade and the other had an absorber integrated within it that was designed to mitigate diametrical chatter. The two thick blades were manufactured by ISCAR and were of the CGHN53-P8 types [23, 24]. GIMY808 inserts with a 0.8 mm radius, and widths of 8 mm were used with both thick blades. The thin blade was manufactured by Ceratizit and was of the XLCFN 3204 M41 FX type [25]. A HW-K15 type insert was used with this blade that had a radius of 0.2 mm and a width of 4.1 mm. Both blades were mounted in their special holders that were procured from their respective manufacturers. The overhang for the thick blades was 130 mm, and for the thin blade, the overhang was 60 mm. We cut Aluminium with all three blades. Feed rate was set to be 0.2 mm/rev for the thick blades, and 0.05 mm/rev for the thin blade. Cutting speeds were varied between 50 m/min and 300 m/min. The experimental setups for cutting with all three blades are shown in Fig. 2(a). A microphone was used to monitor the cutting process signals and data was sampled at a sampling frequency of 51.2 kHz. Data was acquired with CutPro's MALDAQ module [26] using a National Instrument's NI9234 data acquisition device housed in a NI9171 chassis.

Since chatter occurs at frequencies just higher than the natural frequencies of the most flexible elements in a machine tool system [2], natural frequencies of all three

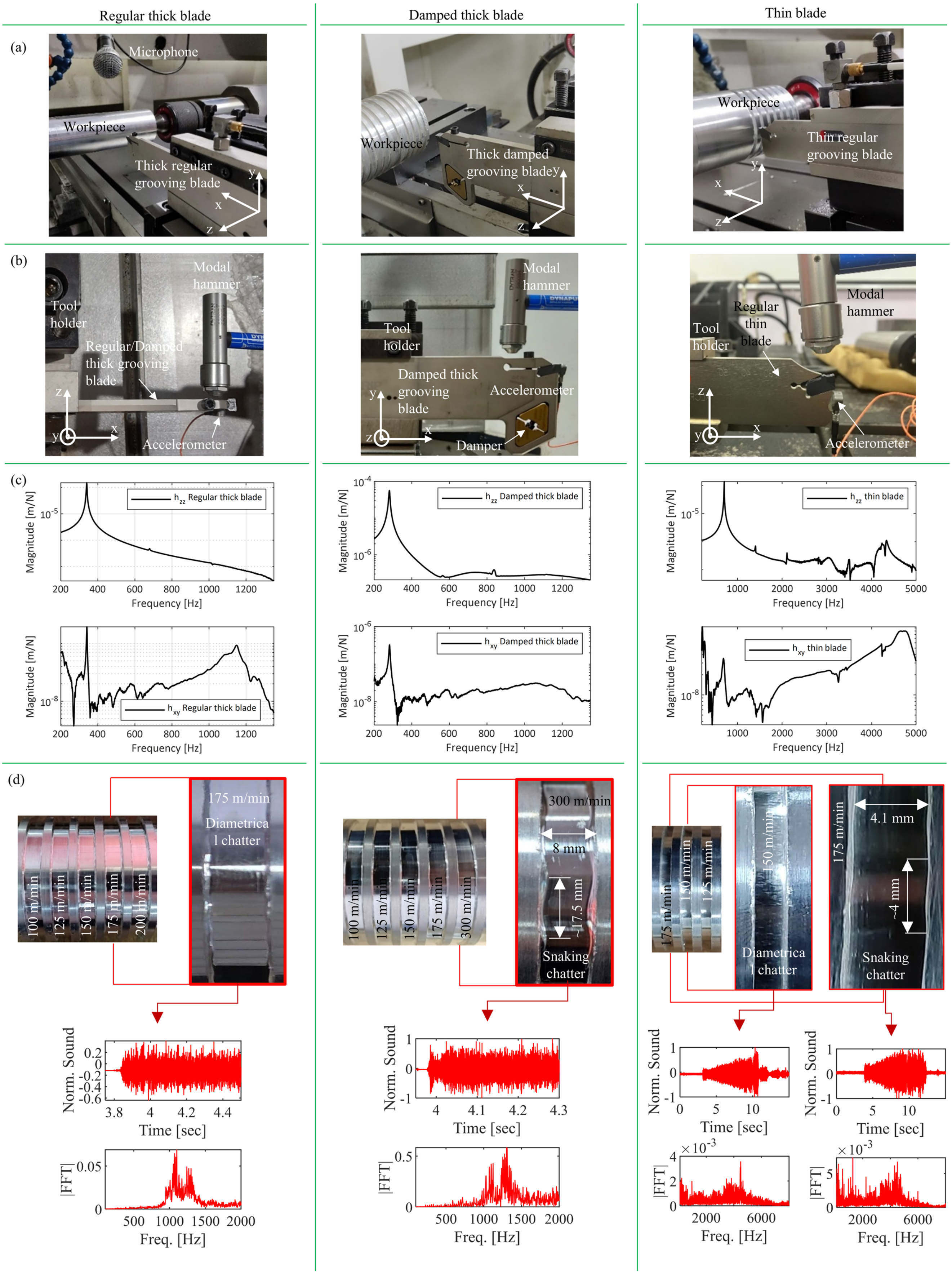

Regular thick blade
Damped thick blade
Thin blade
(a)
Microphone
Workpiece
Thick regular grooving blade
x
y
z
Workpiece
Thick damped grooving blade
Workpiece
Thin regular grooving blade
(b)
Modal hammer
Tool holder
Regular/Damped thick grooving blade
Accelerometer
Modal hammer
Tool holder
Damped thick grooving blade
Accelerometer
Damper
Regular thin blade
Tool holder
Modal hammer
Accelerometer
(c)
Magnitude [m/N]
Frequency [Hz]
h_{zz} Regular thick blade
h_{xy} Regular thick blade
h_{zz} Damped thick blade
h_{xy} Damped thick blade
h_{zz} thin blade
h_{xy} thin blade
(d)
175 m/min
Diametrical chatter
100 m/min
125 m/min
150 m/min
175 m/min
200 m/min
300 m/min
8 mm
~17.5 mm
Snaking chatter
100 m/min
125 m/min
150 m/min
175 m/min
300 m/min
175 m/min
150 m/min
125 m/min
150 m/min
Diametrical chatter
175 m/min
4.1 mm
~4 mm
Snaking chatter
Norm. Sound
Time [sec]
|FFT|
Freq. [Hz]

Fig. 2 (**a**) Pictures of setups for cutting with the three different blades, (**b**) Representative pictures of setups for measuring the in- and out-of-plane dynamics of the three different blades. (**c**) Measured $\boldsymbol{h}_{xy}$ and $\boldsymbol{h}_{zz}$ FRFs of the three blades. (**d**) Representative pictures of machined grooves to show diametrical and snaking chatter supported by the measured sound and its frequency spectrum

blades in the directions of interest were estimated from measurements using setups as shown in Fig. 2(b). Dynamics of the blades were measured by exciting the blade with a modal hammer (make: Dytran, model: 5800B4) and by measuring the response using a single-axis accelerometer (make: Dytran, model: 322F1). Dynamic measurements were done using CutPro's MALTF module [26]. Measurements were carried out to measure the in-plane bending mode by exciting the blades in the y direction and by measuring the response in the x direction. This resulted in the $\boldsymbol{h}_{xy}$ FRFs. Representative setups to measure the $\boldsymbol{h}_{xy}$ FRFs for the thin and thick damped blade are shown in Fig. 2(b). Measurements were also separately conducted to measure the out-of-plane bending modes by exciting and measuring in the z direction. This resulted in the $\boldsymbol{h}_{zz}$ FRFs. A representative setup for measuring the thick regular blade's setup is shown in the Fig. 2(b). For these dynamic measurements too, data was sampled at 51.2 kHz. The same hardware as that used to monitor sound was also used for these measurements.

The measured $\boldsymbol{h}_{xy}$ and $\boldsymbol{h}_{zz}$ FRFs for the three blades are shown in Fig. 2(c). As is evident from the cross $\boldsymbol{h}_{xy}$ FRF of the regular thick blade, there is a low-frequency mode at ~340 Hz and a higher frequency mode at ~1140 Hz. The direct $\boldsymbol{h}_{zz}$ FRF on the other hand has just one low-frequency mode at ~340 Hz. Since the low-frequency mode is common to both measurements and since it is three orders of magnitude more flexible in the z direction than it is in the xy direction, the low-frequency mode is predominantly a bending mode in the z direction with some cross-coupling with the xy direction, whereas the higher frequency mode in the xy direction is simply an in-plane bending mode.

Unlike the regular thick blade, the damped thick blade has just one low-frequency mode at ~280 Hz that is common in the $\boldsymbol{h}_{xy}$ and $\boldsymbol{h}_{zz}$ FRFs. In this case too, since the z directional response is two orders of magnitude higher than the xy direction, the mode is predominantly a bending mode. And, since the damped blade was designed to damp the in-plane xy directional bending mode, there appears to no significant peak at higher frequencies in the xy direction for this blade.

The thin blade too has two modes. One at ~700 Hz in both the $\boldsymbol{h}_{xy}$ and $\boldsymbol{h}_{zz}$ FRFs, and the other between ~4400 Hz and ~4700 Hz only in the xy direction. The mode at ~700 Hz is four orders of magnitude more flexible in the z direction than it is in the xy direction, suggesting that this is indeed the out-of-plane bending mode of the blade. The other higher-frequency mode hence becomes the in-plane bending mode. However, since the input bandwidth was not sufficient, the natural frequency and the peak amplitude of this mode is not correctly estimated.

Representative photographs of cut grooves that show chatter along with the measured sound and its frequency spectra are shown in Fig. 2(d) for all three blades. Since our prior preliminary work already discussed what stable cases look like [3], analysis herein is limited to only the chatter cases. For the thick regular blade, results are shown for cutting with a speed of 175 m/min. For the damped thick blade, results are shown for a speed of 300 m/min. And, for the thin blade, results are shown for cutting at speeds of 150 m/min, and at 175 m/min, respectively.

The diametrical surface cut with the regular blade clearly shows chatter and the spectrum of the sound shows a peak around ~1150 Hz which corresponds to the in-plane bending mode of the blade. Since the damped blade was designed to damp diametrical chatter, no regenerative chatter was observed on the diameter for cutting with the damped blade. However, large undulations on the side walls were observed when cutting with the damped blade. Though the spectrum of the measured (normalized) sound in this case has a cluster of peaks in between 1 and 1.5 kHz, since the damped blade has no modes in this frequency range, attributing chatter to a mode from the spectrum is not possible. Hence, we instead measured the wavelength, λ of the vibration marks left on the side walls of the machined surface and infer the snaking chatter frequency, f_{CS} from the wavelength and the cutting speed, v. Since $v = 2\pi\, f_{\mathrm{CS}} \bullet \lambda$, for cutting at 300 m/min, and λ measuring 17.5 mm, f_{CS} is ~286 Hz. This is just higher than the z directional mode at ~280 Hz, confirming that this is indeed a case of snaking chatter.

For cutting with the thin blade, two separate representative cut surfaces clearly show chatter on the diameter and on the side walls. For the experiment that resulted in chatter on the diameter, the measured (normalized) sound clearly shows a growing tendency suggesting chatter. Though the spectrum is not clean, and even though there are several peaks in the spectrum, there appears a dominant peak around ~4500 Hz that could correspond to the to the in-plane bending mode of this blade. The spectrum for the case of snaking chatter is however inconclusive. Hence, like we did for the thick blade, for this thin blade too we measured the wavelength of the undulations on the side walls of the machined surface to be λ = ~4 mm. For cutting as a speed of 175 m/min, this made the chatter frequency f_{CS} = ~729 Hz, which is higher than the z directional mode at ~700 Hz, confirming that cutting with the thin blade too results in snaking chatter.

Since cutting with the thick and the thin blades were observed to result in two different types of chatter which in turn were caused by two distinct modes of the blade, the next section discusses the integration of two absorbers within the blade to damp the two different modes responsible for the two types of chatter.

Potential Design of a Damped Grooving Blade with Two Absorbers

A schematic of a potential design of a grooving blade integrated with two absorbers is shown in Fig. 3. As an illustrative example, the two absorbers are to be integrated in the ISCAR-made thick regular blade [23] that is already available with us. Absorber I is placed below the cutting edge following the commercially available damped blade design concept, and absorber II is placed as near the front as possible. Absorber I is to damp the in-plane xy bending mode. It consists of a mass supported in an O-ring. Absorber II is to damp the z directional out-of-plane bending mode. Since the second absorber must move out-of-plane, and since O-rings cannot allow this out-of-plane motion, the second absorber's mass is to be supported in flexure bearings that allow lateral motion only [27]. The design task reduces to sizing the mass of both absorbers along with finding the right stiffness and damping properties of the O-ring for absorber I and of the flexure bearing for absorber II.

Our concept design is informed by the standard way to model absorbers for tooling systems in which the absorber is generally modelled as a rigid body supported in a spring-damper [6–10, 12–14].

Receptance Coupling Framework To Integrate Two Tuned Absorbers

This section has three sub-sections. In the first sub-section we present a general framework that shows how the blade's response can be made to be a function of the two absorbers integrated within it. The second sub-section discusses the formulation of an optimization problem that seeks to identify the parameters of the two absorbers that will result in damped response of the blade. And the final sub-section discusses how we obtain the receptances of the blades and of the different absorbers.

Receptance Coupling Framework

Receptance coupling combines the FRFs of subsystems and predicts the assembled system's response. The assembled system in our case is the grooving blade that is subsystem I and that is integrated with two absorbers, that are subsystems II and III, respectively. Assembly of subsystems is shown schematically in Fig. 4. Though the absorbers are attached over a finite area in the design concept shown in Fig. 3, in the model, both absorbers are assumed attached at a point on the blade as shown in the schematic in Fig. 4.

Subsystem II is the absorber to be integrated within the blade to damp regenerative chatter, and subsystem III is the absorber for mitigating snaking chatter. Subsystems II and III each include a mass (m_1 and m_2) connected to

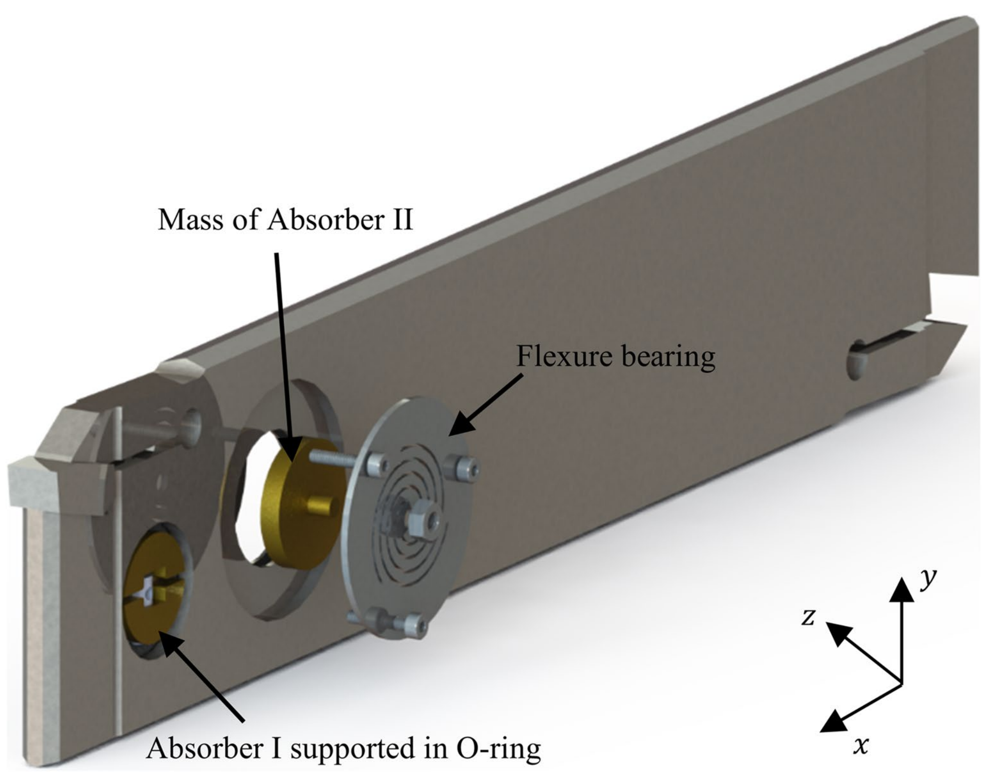

Fig. 3 Schematic of a potential design of two absorbers integrated within a regular thick grooving blade

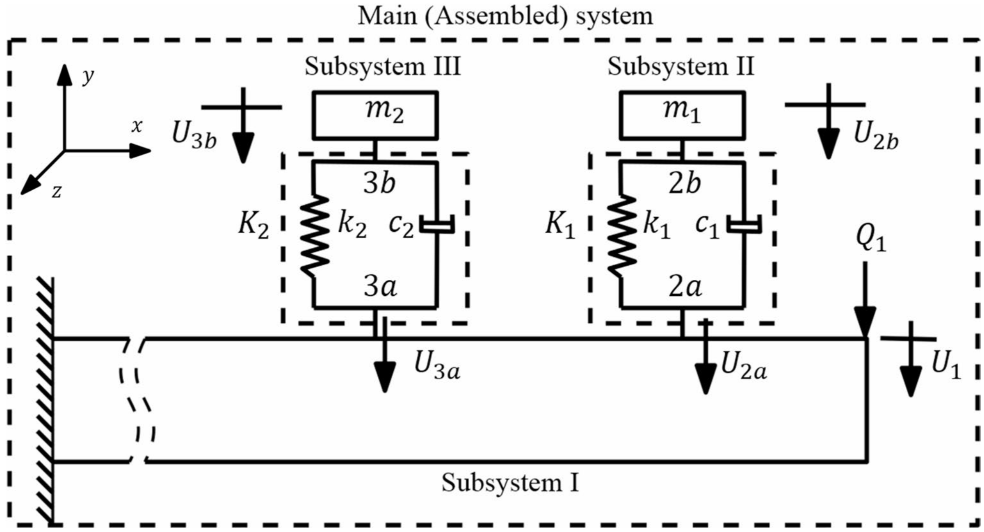

Fig. 4 Schematic of a three subsystems connected to each other

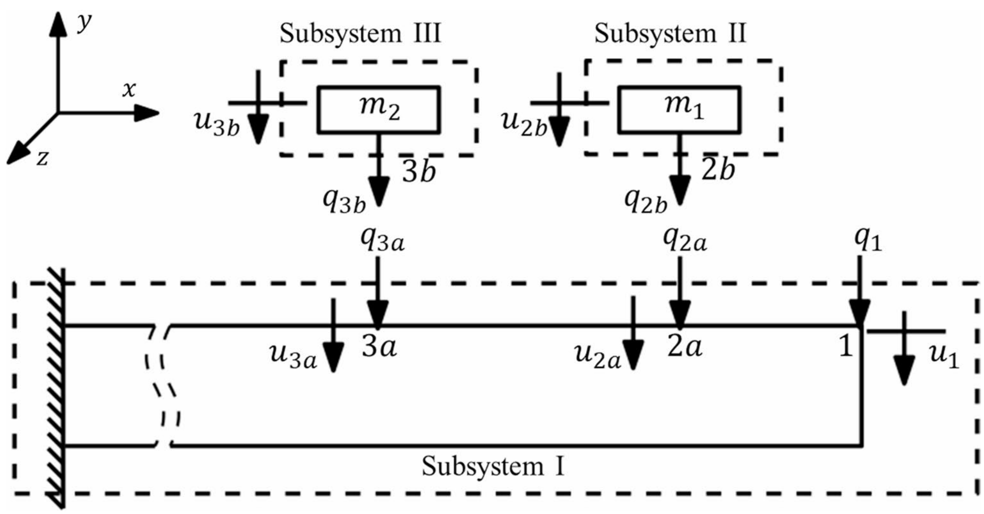

Fig. 5 Schematic showing free-body diagrams of the three subsystems

subsystem I with a spring (k_1 and k_2) and damper (c_1 and c_2). The central idea is to impose compatibility and equilibrium conditions at the connections, i.e., at locations 2 and 3, respectively such as to predict the assembled system response at location 1 as a function of individual subsystems response.

A schematic showing free body diagrams of the different subsystems is in Fig. 5. In it, points $2a$ and $3a$ correspond to points on the blade, and points $2b$ and $3b$ correspond to points on subsystem II and III, respectively. If we assume the displacements of subsystem I at location 1, $2a$, $3a$ are $\boldsymbol{u}_1$, $\boldsymbol{u}_{2a}$, $\boldsymbol{u}_{3a}$, respectively, and forces at those locations are $\boldsymbol{q}_1$, $\boldsymbol{q}_{2a}$, $\boldsymbol{q}_{3a}$ respectively, then likewise, for subsystems II and III, the displacements and forces are $\boldsymbol{u}_{2b}$, $\boldsymbol{u}_{3b}$, and $\boldsymbol{q}_{2b}$, $\boldsymbol{q}_{3b}$, respectively. The displacement and force vectors are bold faced because they contain elements corresponding to all directions, i.e., the x, y, and z directions. The frequency-dependent relationship between displacements ($\boldsymbol{u}$) and forces ($\boldsymbol{q}$) is defined as the receptance, $\boldsymbol{h}(\omega) = \frac{\boldsymbol{u}}{\boldsymbol{q}}$, wherein ω is the frequency vector.

When the force applied and resulting response is considered at the same location, then, the direct FRFs of subsystem I, II and III are designated as $\boldsymbol{h}_{11}$, $\boldsymbol{h}_{2a2a}$, $\boldsymbol{h}_{2b2b}$, $\boldsymbol{h}_{3a3a}$, and $\boldsymbol{h}_{3b3b}$, respectively. Likewise, if the point of application of force and measurement location is different, then the cross FRFs for subsystem I are designated as $\boldsymbol{h}_{12a}$, $\boldsymbol{h}_{13a}$ and $\boldsymbol{h}_{2a3a}$. Since each location can respond to forces in all three directions, i.e., the x, y, and z directions, the generalized response matrix for the direct and cross FRFs including responses between different directions becomes:

$$\boldsymbol{R}_{st} = \begin{bmatrix} \boldsymbol{h}_{s_x t_x} & \boldsymbol{h}_{s_x t_y} & \boldsymbol{h}_{s_x t_z} \\ \boldsymbol{h}_{s_y t_x} & \boldsymbol{h}_{s_y t_y} & \boldsymbol{h}_{s_y t_z} \\ \boldsymbol{h}_{s_z t_x} & \boldsymbol{h}_{s_z t_y} & \boldsymbol{h}_{s_z t_z} \end{bmatrix} \tag{1}$$

wherein s, t are indices that can take on any of the values of 1, $2a$, $3a$, $2b$, and/or $3b$. Each of the elements in the matrix in Eq. (1) is a frequency dependent quantity. However, for the sake of brevity, ω - the frequency vector, is not shown. Also important to note is that since the receptance coupling approach assumes linearity and reciprocity, the generalized response matrix is symmetric, i.e., $\boldsymbol{h}_{s_x t_y} = \boldsymbol{h}_{s_y t_x}$, $\boldsymbol{h}_{s_x t_z} = \boldsymbol{h}_{s_z t_x}$, and $\boldsymbol{h}_{s_y t_z} = \boldsymbol{h}_{s_z t_y}$..

Since most machine tool systems (including one in which a grooving operation will be performed) operate in a small-amplitude elastic regime in which damping is generally low and can be approximated to be proportional to the mass and/or the stiffness, the equations of motion are linear. As such, the system can be modelled with second order ordinary differential equations that form the mathematical basis for the dynamic stiffness matrices. And, since the dynamic stiffness matrices are real, symmetric, and positive definite (for proportionally damped system), their inverse, which are used to obtain receptance matrices, are also real and symmetric – forming the basis for reciprocity holding true.

The form of the response at location $\boldsymbol{u}_1$ due to forces at the same and different locations is:

$$\boldsymbol{u}_1 = \boldsymbol{R}_{11}\boldsymbol{q}_1 + \boldsymbol{R}_{12a}\boldsymbol{q}_{2a} + \boldsymbol{R}_{13a}\boldsymbol{q}_{3a}. \tag{2}$$

Likewise, for locations $2a$ and $3a$, the responses are:

$$\begin{aligned} u_{2a} &= R_{2a1}q_1 + R_{2a2a}q_{2a} + R_{2a3a}q_{3a} \; and \\ u_{3a} &= R_{3a1}q_1 + R_{3a2a}q_{2a} + R_{3a3a}q_{3a}, \end{aligned} \tag{3}$$

And for locations $2b$ and $3b$, the responses are:

$$\boldsymbol{u}_{2b} = \boldsymbol{R}_{2b2b}\boldsymbol{q}_{2b} \text{ and } \boldsymbol{u}_{3b} = \boldsymbol{R}_{3b3b}\boldsymbol{q}_{3b}. \tag{4}$$

Above responses are obtained at the subsystem level. To obtain the assembled system response, we must satisfy the following compatibility and equilibrium conditions at the connections, i.e., in between $2a$ and $2b$, and in between $3a$ and $3b$. Since the connections between the mass of both absorbers and the blade is through springs and dampers, the compatibility conditions can be expressed though a complex stiffness function $k\prime = k + ic\omega$, such that:

$$\boldsymbol{K}_1' (\boldsymbol{u}_{2a} - \boldsymbol{u}_{2b}) = -\boldsymbol{q}_{2a} \text{ and } \boldsymbol{K}_2' (\boldsymbol{u}_{3a} - \boldsymbol{u}_{3b}) = -\boldsymbol{q}_{3a}. \tag{5}$$

wherein $\boldsymbol{K}_1'$ and $\boldsymbol{K}_2'$ are matrices whose elements include complex stiffnesses in the different x, y, and z directions, respectively.

The equilibrium force conditions at the connections are:

$$\boldsymbol{q}_{2a} + \boldsymbol{q}_{2b} = 0, \text{ and } \boldsymbol{q}_{3a} + \boldsymbol{q}_{3b} = 0, \tag{6}$$

and, at the free end the force equilibrium condition is $\boldsymbol{q}_1 = \boldsymbol{Q}_1$, wherein the uppercase corresponds to the force on the assembled system. Since we couple substructures that are linear, the interactions during coupling are also governed by the same linearity and reciprocity.

The assembled system response at location 1 can hence be written as the relationship between the force acting at location 1, i.e., $\boldsymbol{q}_1 = \boldsymbol{Q}_1$ and the response at the same location, i.e., $\boldsymbol{u}_1 = \boldsymbol{U}_1$. Equation (2) can be used to describe $\boldsymbol{u}_1$ to show that the assembly receptance becomes:

$$\boldsymbol{G} = \frac{\boldsymbol{U}_1}{\boldsymbol{Q}_1} = \frac{\boldsymbol{u}_1}{\boldsymbol{Q}_1} = \boldsymbol{R}_{11}\left(\frac{\boldsymbol{q}_1}{\boldsymbol{Q}_1}\right) + \boldsymbol{R}_{12a}\left(\frac{\boldsymbol{q}_{2a}}{\boldsymbol{Q}_1}\right) + \boldsymbol{R}_{13a}\left(\frac{\boldsymbol{q}_{3a}}{\boldsymbol{Q}_1}\right). \tag{7}$$

The above equation shows the response to be a function of direct and cross receptances of only subsystem I. However, since we desire to develop an expression in which the response at the free end of the blade is a function of the absorber parameters, we develop an alternate form for $\boldsymbol{G}$ as follows.

For absorber I, i.e., for subsystem II, we use the compatibility condition in Eq. (5), the force equilibrium in Eq. (6), and the response from Eq. (3) and Eq. (4), to obtain:

$$\boldsymbol{R}_{2a1}\boldsymbol{q}_1 + \left(\boldsymbol{R}_{2a2a} + \boldsymbol{R}_{2b2b} + \frac{1}{\boldsymbol{K}_1'}\right)\boldsymbol{q}_{2a} + \boldsymbol{R}_{2a3a}\boldsymbol{q}_{3a} = 0, \tag{8}$$

wherein $\boldsymbol{R}_{2a1}$ is the same $\boldsymbol{R}_{12a}$ in Eq. (7). Likewise, for absorber II, i.e., for subsystem III, we can show that:

$$\boldsymbol{R}_{3a1}\boldsymbol{q}_1 + \left(\boldsymbol{R}_{3a3a} + \boldsymbol{R}_{3b3b} + \frac{1}{\boldsymbol{K}_2'}\right)\boldsymbol{q}_{3a} + \boldsymbol{R}_{3a2a}\boldsymbol{q}_{2a} = 0, \tag{9}$$

wherein $\boldsymbol{R}_{3a1}$ is the same $\boldsymbol{R}_{13a}$ in Eq. (7). Grouping like terms common to Eq. (7), Eq. (8), and Eq. (9), it is easy to show that, the assembled system response becomes:

$$\begin{aligned} &G = R_{11} - [R_{12a} \; R_{13a}] \\ &\begin{bmatrix} R_{2a2a} + R_{2b2b} + \frac{1}{K_1'} & R_{2a3a} \\ R_{3a2a} & R_{3a3a} + R_{3b3b} + \frac{1}{K_1'} \end{bmatrix}^{-1} \begin{bmatrix} R_{2a1} \\ R_{3a1} \end{bmatrix}, \end{aligned} \tag{10}$$

which shows the assembled systems response to be a function of the blade's response in terms of the direct and cross receptances of the blade, i.e., of $\boldsymbol{R}_{11}$, $\boldsymbol{R}_{2a2a}$, $\boldsymbol{R}_{3a3a}$, $\boldsymbol{R}_{12a}$, $\boldsymbol{R}_{13a}$, and $\boldsymbol{R}_{2a3a}$, respectively and of both the absorber's system responses, i.e., of $\boldsymbol{R}_{2b2b}$ and $\boldsymbol{K}_1'$ for absorber I and of $\boldsymbol{R}_{3b3b}$ and $\boldsymbol{K}_2'$ for absorber II.

Structure of $\boldsymbol{G}$ is:

$$\boldsymbol{G} = \begin{bmatrix} \boldsymbol{h}_{xx} & \boldsymbol{h}_{xy} & \boldsymbol{h}_{xz} \\ \boldsymbol{h}_{yx} & \boldsymbol{h}_{yy} & \boldsymbol{h}_{yz} \\ \boldsymbol{h}_{zx} & \boldsymbol{h}_{zy} & \boldsymbol{h}_{zz} \end{bmatrix} \tag{11}$$

wherein the only responses of interest are the cross receptance $\boldsymbol{h}_{xy}$ that corresponds to the in-plane bending mode of the plate responsible for diametrical chatter and the direct receptance $\boldsymbol{h}_{zz}$ that corresponds to the out-of-plane bending mode of the plate that is responsible for snaking chatter.

Setting Up the Optimization Problem

Since the aim is to develop a damped blade that has two absorbers that can damp the two separate modes responsible for the two types of chatter that is observed, and since the likelihood of the occurrence of chatter is inversely proportional to how flexible the blade is [2, 12, 20], we setup an optimization problem that aims to minimize the peak amplitude of the dominant modes in the $|\boldsymbol{h}_{xy}|$ and the $|\boldsymbol{h}_{zz}|$ FRFs. Since the blade with two absorbers must damp both modes, the logical choice for an objective function is to minimize the sum of the square root of $\boldsymbol{h}_{xy}$ and $\boldsymbol{h}_{zz}$:

$$\min(\boldsymbol{G}_{objs} = \sqrt{(\boldsymbol{h}_{xy}^2 + \boldsymbol{h}_{zz}^2)}) \text{ such that } \begin{cases} 0 \leq \zeta \leq 1 \\ 0 \leq k \leq \infty \\ lb \leq m_{\text{II, III}} \leq ub \end{cases} \tag{12}$$

wherein k is the stiffness, $m_{1,\,2}$ is the mass of tuned mass dampers of subsystem II or III and for which lb and ub are the lower and upper bounds, respectively, and ζ is damping ratio that is related to the damping coefficient, the stiffness, and the mass, such that: $\zeta = \frac{c}{2\sqrt{km}}$. Given the blade's receptances, the optimum parameters of the absorbers can be found using one of the many optimization routines. In this work, we prefer the simplex-based direct search method of Lagarias et al. [28] which we implement using the *fminsearch* function in MATLAB.

Obtaining the Subsystem Level Receptances

Since the aim of this work is to demonstrate the method of integrating two absorbers within a blade, we rely on numerical methods to obtain receptances for the blade and the absorber's mass. For the blade, we build a finite element model. And, for the absorber masses, we use a rigid body approximation of the mass.

A 3D CAD model of the blade as shown in Fig. 3 was imported into the finite element environment for modelling it and obtaining its response. The blade is modelled in the ANSYS environment using 10-noded tetrahedral elements that have three degrees of freedom at each node. The blade is assumed made of alloyed steel with a modulus of 200,000 N/mm^2, a density of 7850 kg/m^3, and with a Poisson's ratio of 0.3. The blade's thickness is 7.4 mm, height is 50 mm, and its overhang is 120 mm. Since the blade is usually rigidly clamped in special holders, the top and bottom clamping surfaces of the blade are assumed fixed in the model, i.e., displacements on those nodes are set to be zero. This is shown in in Fig. 6. Two holes are made in the blade to house the two absorbers. Different diameters were tried, but since larger holes weakened the blade, and since holes with a diameter of 20 mm only reduced the static stiffness of the blade by ~15%, the hole diameters were fixed to be 20 mm.

Since the receptance coupling approach assumed that the absorbers are to be connected to the blade at single attachment points, we introduce a node in the centre of both holes in the blade and connect those nodes to the inner surface of the holes in the blades using rigid link elements [29]. This allows us to extract the receptances at the two coupling points, i.e., at locations $2a$ and $3a$, respectively, and at the free end, i.e., at location 1. To obtain the receptances at these three locations, we solve the eigenvalue problem and extract the eigenvalues (natural frequencies) and the eigenvectors (mode shapes). With these, we obtain the in-plane ($\boldsymbol{h}_{s_x t_y}$) and out-of-plane ($\boldsymbol{h}_{s_z t_z}$) receptances using:

$$\begin{aligned} h_{s_x t_y}(\omega) &= \sum \omega \sum_{r=1}^{n} \frac{\varphi_{s_x r}\varphi_{t_y r}}{-\omega^2 + \omega_{n_r}^2 + 2j\zeta_r \omega\,\omega_{n_r}}, \\ hs_z t_z(\omega) &= \sum \omega \sum_{r=1}^{n} \frac{\varphi_{s_z r}\varphi_{t_z r}}{-\omega^2 + \omega_{n_r}^2 + 2j\zeta_r \omega\,\omega_{n_r}} \end{aligned} \tag{13}$$

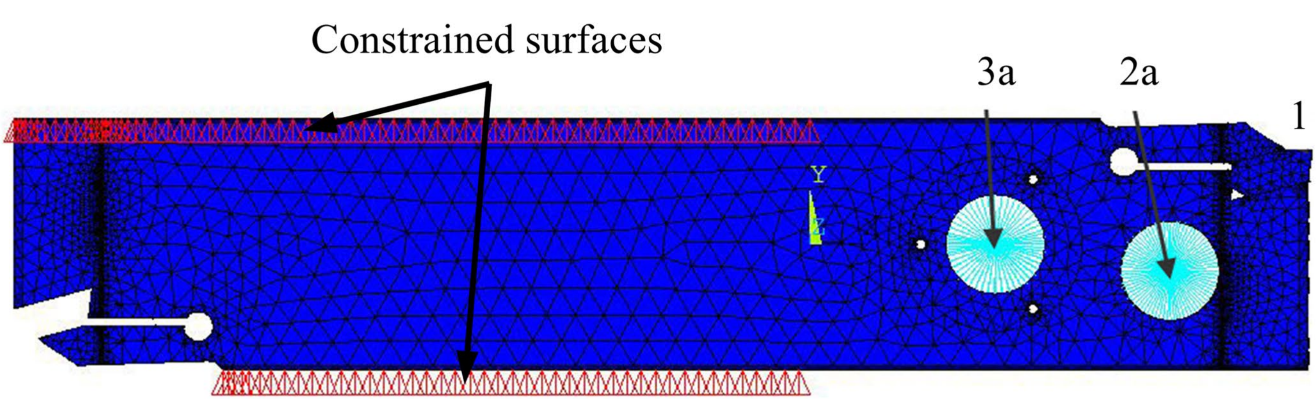

Fig. 6 Finite element model representation of the blade with two holes to accommodate two absorbers

wherein s is the response location that can be any of the locations 1, $2a$, or $3a$, and the excitation location t can also be any of the locations 1, $2a$, or $3a$. $\varphi_{s_x r}$, $\varphi_{t_y r}$, $\varphi_{s_z r}$, and $\varphi_{t_z r}$ are the mass normalized eigenvectors for mode r, and ζ_r and ω_{nr} are the damping ratios and natural frequencies for mode of interest r. For the blade's receptances, we assume the damping ratio for all modes to be 1%, i.e., $\zeta_r = 0.01$. Since experimental analysis of the modes contributing to chatter suggest that modes of interest lie below 1500 Hz, in our simulations, we hence include all modes up to 3000 Hz.

For the mass of both absorbers that we approximate as a rigid body, the receptance is more straightforward:

$$\boldsymbol{h}_{s_x t_y}(\omega) = \sum \omega \frac{-1}{m\omega^2} \tag{14}$$

wherein s and t both correspond to locations $2b$ or $3b$, and $m_{1,\,2}$ is mass of tuned mass dampers of subsystem II or III. These subsystem level receptances are combined to find the damped response of the blade integrated with two absorbers using the optimization procedure above. Results are discussed in the next section.

Damped Response of the Blade with Two Absorbers

The assembled system response is predicted herein by combining subsystem level receptances. Since it has previously been established that the absorber's mass should be as high as possible to improve the absorber's vibration absorption capacity [11, 12, 20], we assume that the absorber is made of a heavy material such as tungsten carbide that has a density of 15,630 kg/m^3. Since the width of the blade is fixed, and since the two holes to locate absorbers also have a fixed size, the mass of both absorbers is evaluated to be 0.04 kg each. The optimization problem hence reduces to finding the stiffness and damping of the two connection elements of the two absorbers that minimizes: $\sqrt{(\boldsymbol{h}_{xy}^2 + \boldsymbol{h}_{zz}^2)}$. Results obtained are summarized in Fig. 7 for the in-plane xy mode, and in Fig. 8 for the out-of-plane z-directional mode.

Both figures show subsystem level receptances as well as the assembled system response with two tuned absorbers and compare that with the response without dampers. The assembled system response is shown only at the free end, i.e., at location 1 which is also the cutting end.

As is evident from Fig. 7(a), the subsystem level response at the free end, i.e., $\boldsymbol{h}_{1_x 1_y}$ is the most flexible, and the cross FRFs between locations 1 and $2a$, i.e., $\boldsymbol{h}_{1_x 2a_y}$, and between locations 1 and $3a$, i.e., $\boldsymbol{h}_{1_x 3a_y}$ are dynamically stiffer. The direct FRF at location $2a$, i.e., $\boldsymbol{h}_{2a_x 2a_y}$ is most stiff. All these responses have just a single mode corresponding to the in-plane xy being mode. This mode has a natural frequency of 1261 Hz. Since the absorber's mass is modelled as a rigid body, its response, i.e., $\boldsymbol{h}_{2b2b}$ is like that of a rigid body, i.e., with a negative slope.

Assembling the receptances shown in Fig. 7(a) using Eq. (10) and solving the optimization problem defined in Eq. (12), we find that a stiffness of 0.13×10^6 N/m and a damping ratio of 0.27 for absorber I minimizes the assembled system response. These stiffness and damping values are typical of soft elastomers that are used to support dampers in tooling systems [30].

The peak magnitude of the assembled system response with these parameters that is shown in Fig. 7(b) is ~53% less than the peak magnitude of the response of the blade without a damper – suggesting that the absorber we have integrated and tuned indeed has the potential to damp the in-plane xy bending mode that is responsible for diametrical chatter. The natural frequency for the damped blade is 1219 Hz, which is 42 Hz lower than the blade without dampers. This too is consistent with what damping does to natural frequencies.

Like Fig. 7 shows the response for the in-plane xy mode, Fig. 8 shows the response for the out-of-plane z-directional mode. As is evident from Fig. 8(a), all receptances in the z -direction have multiple modes. The first mode at 376 Hz has the highest magnitude and is two orders of magnitude more flexible than the in-plane xy mode shown in Fig. 7. Since this behavior is like what we measured for the original thick blade (see Fig. 2), it is safe to assume that this low-frequency mode is indeed the out-of-plane z-directional mode. The second mode seen in Fig. 8(a) has a natural frequency close to the xy mode, suggesting that there is cross-coupling between directions. The third mode at ~2375 Hz is dynamically stiffer than the first mode by two orders of magnitude and is hence thought to be of little consequence in governing the out-of-plane response of the blade. In this case too, the subsystem level direct FRF at location 1, i.e., $\boldsymbol{h}_{1_z 1_z}$ is significantly more flexible than the cross FRFs between locations 1 and $2a$, i.e., $\boldsymbol{h}_{1_z 2a_z}$, and between locations 1 and $3a$, i.e., $\boldsymbol{h}_{1_z 3a_z}$. The $\boldsymbol{h}_{1_z 1_z}$ FRF is also more flexible than the direct FRF at location $3a$, i.e., $\boldsymbol{h}_{3a_z 3a_z}$. The subsystem level response of absorber II is like absorber I.

When the subsystem level receptances shown in Fig. 8(a) are assembled and the optimization problem is solved, the stiffness and damping ratio of absorber II that minimizes the response are found to be of 3.79×10^6 N/m and 0.38, respectively. Since our design for absorber II assumes it to be supported in flexure bearings that are usually made of spring steel [27], it is interesting that the tuned stiffness value for absorber II is an order higher than the stiffness of the absorber I which we assume will be supported in elastomeric O-rings. With these tuned absorber II parameters,

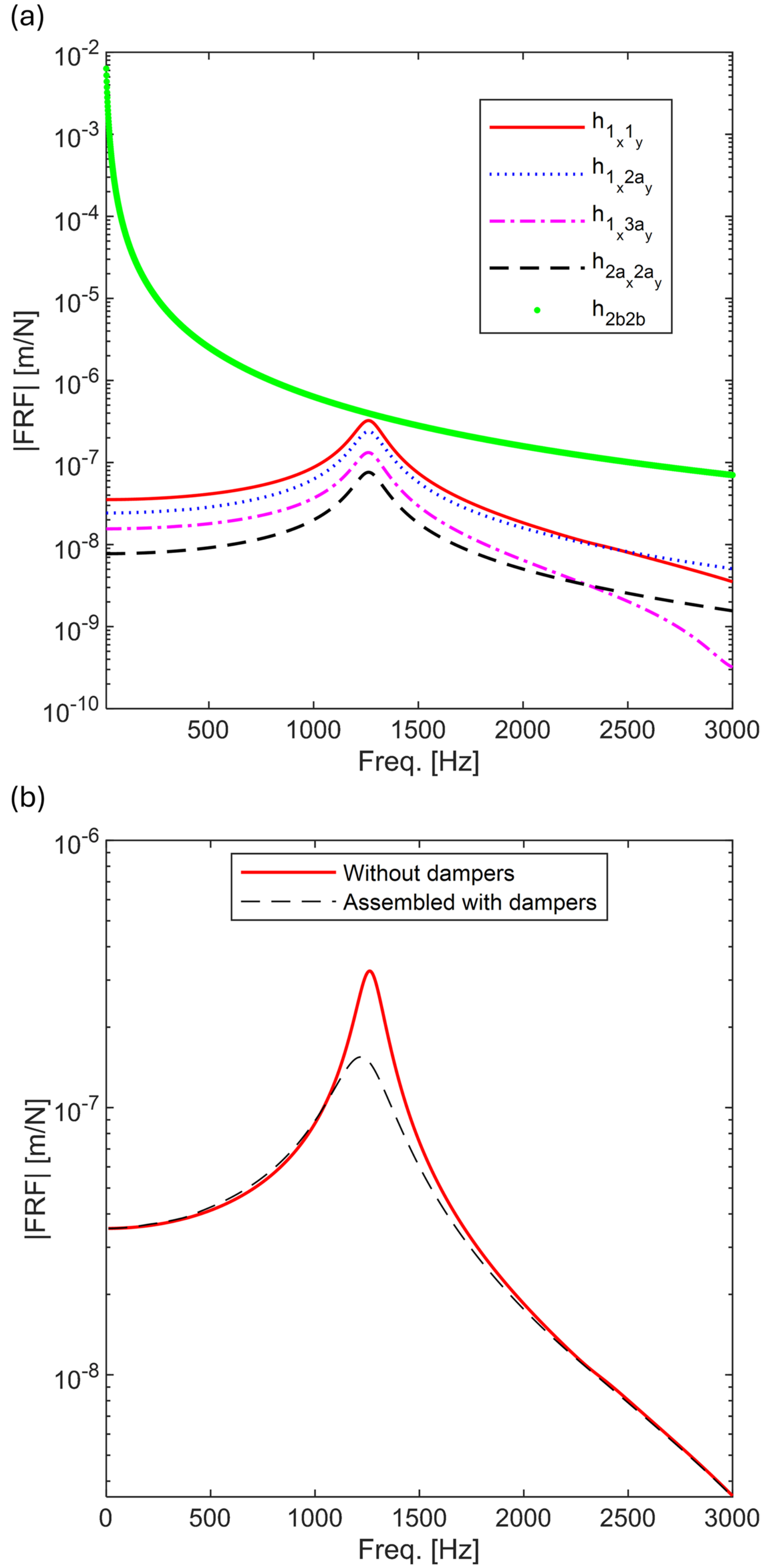

Fig. 7 (**a**) Subsystem level receptances for the in-plane xy mode, and (**b**) tool point assembled in-plane xy FRF with and without integrating two tuned absorbers

Fig. 8 (**a**) Subsystem level receptances for the out-of-plane z-directional mode, and (**b**) tool point assembled out-of-plane z-directional FRF with and without integrating two tuned absorbers

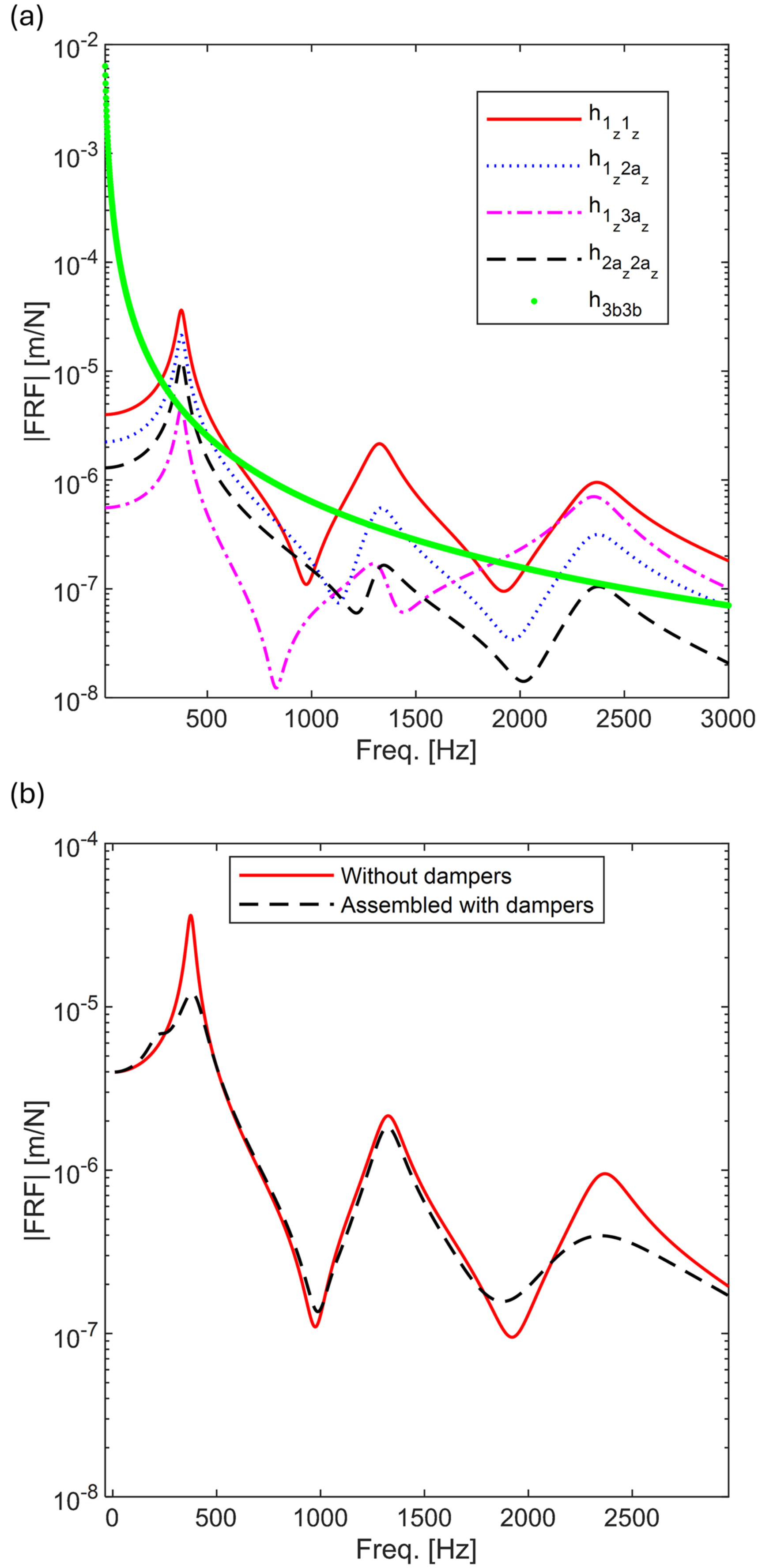

we find that the peak amplitude of the out-of-plane low-frequency z-directional mode shown in Fig. 8(b) reduces by ~ 67% in comparison to the blade without dampers. Interestingly, the ~ 1262 Hz mode that corresponds to the in-plane xy mode is also damped by 15%. This confirms that the absorber integrated to damp the out-of-plane mode does not inadvertently exacerbate coupling with the in-plane mode but helps damp that mode too. The higher frequency mode at ~ 2370 Hz is damped significantly too. This suggests that the higher frequency mode too is an out-of-plane z-directional mode. These results suggest that the out-of-plane z-directional mode(s) that are responsible for snaking chatter can be damped with the second tuned absorber that we have integrated into the blade.

Discussions

This section discusses aspects of the design and methodology that could affect performance of the proposed solution. We first discuss the role of holes made within the blade, followed by design aspects of the absorbers. That in turn in followed by the role of changing absorber mass on the damping performance. We finally discuss how solutions are influenced by changing the objective function.

On the role of holes in the blade to integrate the absorbers: Though holes weaken the blade, they are necessary to integrate the absorbers within the blade. Such cavities are common in all tools with absorbers integrated within them [6–10]. Moreover, since the chatter-vibration-free process stability is governed more by the dynamic stiffness than by the static stiffness [6–10], and since we demonstrate that the dynamic stiffness can indeed be improved by integrating absorbers, the potential weakening of the blades due to holes is not expected to adversely affect blade performance. Nevertheless, alternate design concepts that do not statically weaken the blade could be explored in future follow-on research. And, once design guides prototyping, it would be prudent to also test for changes in static stiffness, if any.

On the design and selection aspects of the O-rings and flexure bearings: For the absorber integrated to damp the in-plane mode, model suggested stiffness and damping of the elastomer supporting the absorber's mass could be used to guide selection of O-rings from catalogues. Additionally, it should be noted that our design includes an adjustment arrangement that could be used to tune the stiffness of the O-rings as necessary. And, for the absorber for the out-of-plane mode, it should be noted that though our model predictions recommend the optimal stiffness and damping properties for the flexural bearing system, the design and experimental characterization of flexure bearings is non-trivial. Performance of such bearings is governed by their material, their size and geometry, operational temperature, and by cutting fluid potentially hastening rusting and material behavior. Moreover since such bearings work by elastic deformation, the stress concentration due to the slots will undoubtedly influence their fatigue life. Optimal design of such bearings is usually informed by parametric investigations guided by finite element analysis [27]. Moreover, experimental validation of the stiffness and fatigue behavior of such systems requires dedicated setups. Such characterization is beyond the scope of this paper.

On the role of the mass of the absorber: In general, tuned-mass dampers perform better when the mass of the absorber is higher [Ref. 11], and this is also what we had observed in our investigations. Since we have limited space in which to integrate the two absorbers, for the size allowed, we selected a material with higher density. The mass was hence taken to be fixed at 0.04 kg, and with this, the reduction in peak magnitudes of the two modes of interest were evaluated to be ~53% and ~67% respectively, for the in-plane and out-of-plane modes. However, if the two absorbers were assumed to be made of steel instead of Tungsten carbide, the mass of each would become ~0.02 kg each. For the lower absorber mass of 0.02 kg, the 'optimal' stiffness and damping values for the two absorbers were found to be different than the case of 0.04 kg. And the maximum reduction in the peak magnitudes of the FRFs were evaluated to be ~42% and ~55% for the in-plane and out-of-plane modes, respectively, i.e., lesser than the case of the absorber mass being 0.04 kg.

On the role of different objective functions influencing results: Instead of minimizing the sum of the square root of the two FRFs of interest representing the in-plane and out-of-plane modes – as we have done and reported on, we also explored alternative formulations for the objective function in which we tried minimizing individual mode amplitudes separately, i.e., ($\min(\boldsymbol{G}_{objs} = \boldsymbol{h}_{xy})$ or $\min(\boldsymbol{G}_{objs} = \boldsymbol{h}_{zz})$). Our analysis suggested that the best choice for damping a particular mode in a particular direction is to use the objective function formulated to minimize the FRF only in that direction. However, the other mode in the other direction does not get optimally damped while doing this. We hence think it best to use an objective function that minimizes the sum of the square root of the two FRFs even though it results in a slight trade-off over the case of minimizing individual modes.

Conclusions and Outlook

A new multi-absorber tuning framework based on the receptance coupling approach was proposed to damp the two different modes responsible for the two different types of chatter observed in grooving with slender blades. Our proposed approach was shown capable of tuning absorbers to damp different modes in different directions. Thus, overcoming limitations of other methods in the literature that were limited to tuning absorbers to damp different modes in a single direction.

The blade and the two absorbers were treated as three separate subsystems that were assembled using spring and damper connections, parameters of which were found by minimizing the assembled system's response. Simulation-based analysis with these parameters showed that the peak magnitude of the in-plane bending mode can be damped by 53%, and that the peak magnitude of the out-of-plane bending mode can be damped by 67%.

Our design concept and tuning methodology are novel. The absorber parameters we identified are realistic, and the simulation-based results are promising. Together, these support the design, development, and prototyping of new damped blades integrated with two absorbers. We clarify that the present work is intended as a methodological contribution, establishing a new multi-absorber tuning framework and demonstrating its potential through simulations. Experimental prototyping and testing, including optimal design and testing of flexure bearings, are planned for future studies. We further take this opportunity to clarify that the method we propose is not restricted to tooling systems. The method is easily extendable to other systems requiring the integration of multiple absorbers.

Acknowledgements Authors gratefully acknowledge support from the Government of India's Department of Science & Technology's grant on technology development via grant number DST/TDT/AM/2022/148.

Declarations

Competing Interest The authors declare that they have no known competing financial interests or personal relationships that could have appeared to influence the work reported in this paper.

References

1. Siddhpura M, Paurobally R (2012) A review of chatter vibration research in turning. Int J Mach Tools Manuf 61:27–47. https://doi.org/10.1016/j.ijmachtools.2012.05.007
2. Altintas Y, Weck M (2004) Chatter stability of metal cutting and grinding. CIRP Ann 53:619–642. https://doi.org/10.1016/S0007-8506(07)60032-8
3. Jakhar D, Law M (2023) Experimental analysis of chatter in grooving with slender blades. Manuf Lett 38:74–78. https://doi.org/10.1016/j.mfglet.2023.10.001
4. Stone B (2014) Chatter and machine tools. Springer
5. Celikag H, Ozturk E, Sims ND (2021) Can mode coupling chatter happen in milling? Int J Mach Tools Manufact 165:103738. https://doi.org/10.1016/j.ijmachtools.2021.103738
6. Saffury J (2017) Chatter suppression of external grooving tools. Proc CIRP 58:216–221. https://doi.org/10.1016/j.procir.2017.03.215
7. Rivin EI, Kang H (1992) Enhancement of dynamic stability of cantilever tooling structures. Int J Mach Tools Manuf 32:539–561. https://doi.org/10.1016/0890-6955(92)90044-h
8. Tarng YS, Kao J, Lee E (2000) Chatter suppression in turning operations with a tuned vibration absorber. J Mater Process Technol 105:55–60. https://doi.org/10.1016/s0924-0136(00)00585-9
9. Sørby K (2016) Development and optimization of vibration-damped tool holders for high length-to-diameter boring operations. High Speed Mach 2:51–58. https://doi.org/10.1515/hsm-2016-0005
10. Patel A, Yadav A, Law M (2023) Damped chatter resistant boring bar integrated with an absorber working in conjunction with an eddy current damper. J Vib Eng Technol 11:2013–2024. https://doi.org/10.1007/s42417-022-00684-9
11. Den Hartog JP, Ormondroyd J (1928) The theory of the dynamic vibration absorbers. ASME J Appl Mech 50:11–22
12. Sims N (2007) Vibration absorbers for chatter suppression: a new analytical tuning methodology. J Sound Vib 301:592–607. https://doi.org/10.1016/j.jsv.2006.10.020
13. Yang Y, Muñoa J, Altintas Y (2010) Optimization of multiple tuned mass dampers to suppress machine tool chatter. Int J Mach Tools Manuf 50:834–842. https://doi.org/10.1016/j.ijmachtools.2010.04.011
14. Yang Y, Dai W, Liu Q (2015) Design and implementation of two-degree-of-freedom tuned mass damper in milling vibration mitigation. J Sound Vib 335:78–88. https://doi.org/10.1016/j.jsv.2014.09.032
15. Baduidana M, Kenfack-Jiotsa A (2024) Minimization of the primary structure response under random excitation using high-performance passive tuned mass damper ineter control configurations. J Vib Eng Technol 12:37–47. https://doi.org/10.1007/s42417-022-00825-0
16. Schmitz T, Donalson R (2000) Predicting high speed machining dynamics by substructure analysis. CIRP Ann 49:303–308. https://doi.org/10.1016/s0007-8506(07)62951-5
17. Park SS, Altintas Y, Movahhedy M (2003) Receptance coupling for end mills. Int J Mach Tools Manuf 43:889–896. https://doi.org/10.1016/s0890-6955(03)00088-9
18. Law M, Rentzsch H, Ihlenfeldt S (2016) Predicting mobile machine tool dynamics by experimental dynamic substructuring. Int J Mach Tools Manuf 108:127–134. https://doi.org/10.1016/j.ijmachtools.2016.06.006
19. Hamedi B, Taheri S (2025) Theoretical framework for developing a full vehicle hybrid model to predict tire characteristics using receptance coupling technique. J Vib Eng Technol 13:84. https://doi.org/10.1007/s42417-024-01548-0
20. Nagesh S, Law M (2019) Machine tool design with preferentially asymmetrical structures to improve dynamics and productivity. Proc CIRP 79:592–595. https://doi.org/10.1016/j.procir.2019.02.086
21. Yadav A, Talaviya D, Bansal A, Law M (2020) Design of chatter-resistant damped boring bars using a receptance coupling approach. J Manuf Mater Process 4:53. https://doi.org/10.3390/jmmp4020053
22. Ma W, Yang Y, Jin X (2021) Chatter suppression in micro-milling using shank-mounted two-DOF tuned mass damper. Precis Eng 72:144–157. https://doi.org/10.1016/j.precisioneng.2021.04.017
23. ISCAR regular grooving blade (2025) Available online: https://www.iscar.com/eCatalog/Item.aspx?cat=2860058&fnum=45&mapp=TG&GFSTYP=M&srch=1 (Accessed 4th Feb

24. ISCAR anti-vibration grooving blade (2025) Available online: https://www.iscar.com/eCatalog/Family.aspx?fnum=4004&mapp=TG&app=172&GFSTYP=M (Accessed 4th Feb
25. Ceratizit regular grooving blade (2025) Available online: https://toolsunited.com/EN/Article/Details/24696400130734462?dataSource=toolsUnited&print=False (Accessed 4th Feb
26. CutPro Simulation Software—MAL Inc (2025) Available online: https://www.malinc.com/products/cutpro (Accessed 4th Feb
27. Riyaz MD, Dabade BM (2021) Design, analysis and development of flexure bearing for linear compressor. Mater Today Proc 45:2849–2855. https://doi.org/10.1016/j.matpr.2020.11.809
28. Lagarias JC, Reeds JA, Wright MH, Wright PE (1998) Convergence properties of the Nelder-Mead simplex method in low dimensions. SIAM J Optim 9:112–147. https://doi.org/10.1137/S1052623496303470
29. Mechanical ANSYS (2025) APDL Multibody Analysis GuideAccessed 7th Feb
30. Smalley AJ (1977) Stiffness and damping of elastomeric O-ring bearing mounts. NASA-CR-135328